


Research Article

Optimal Damper Slip Force for Vibration Control Structures Incorporating Friction Device with Sway-Rocking Motion Obtained Using Shaking Table Tests

Kazutaka Shirai ¹, Akari Nagaoka,² Nami Fujita,² and Takeshi Fujimori³

¹Faculty of Engineering, Hokkaido University, Sapporo 060-8628, Japan

²Graduate School of Engineering, Hokkaido University, Sapporo 060-8628, Japan

³Technical Research Institute, Obayashi Corporation, Kiyose 204-8558, Japan

Correspondence should be addressed to Kazutaka Shirai; shirai.kazutaka@eng.hokudai.ac.jp

Received 5 November 2018; Revised 20 December 2018; Accepted 23 December 2018; Published 3 February 2019

Academic Editor: Constantin Chalioris

Copyright © 2019 Kazutaka Shirai et al. This is an open access article distributed under the Creative Commons Attribution License, which permits unrestricted use, distribution, and reproduction in any medium, provided the original work is properly cited.

In this study, a series of shaking table tests were conducted using a specimen that consisted of a superstructure, incorporating a friction device and a sway-rocking mechanism under the superstructure to determine the optimal damper slip force of a passive vibration control system considering the effects of sway-rocking motion. The adopted simple friction device, composed of rubber bands and stainless steel plates, allowed the magnitude of the slip force to be easily set. The optimal slip force of the friction device, which minimizes the peak and root-mean-square response of the superstructure subjected to earthquakes, was determined from the shaking table tests. Based on the results, the optimal slip force of the friction device was found to vary according to the input level of the ground motions and the sway-rocking conditions. The obtained results suggest that the effect of sway-rocking motion should be considered in the design of passive control structures and the determination of their optimal damper slip force.

1. Introduction

Passive vibration control, achieved by incorporating supplemental devices such as friction dampers, is an effective approach for increasing energy absorption and thus reducing the dynamic response and damage of structures during earthquakes. To date, many studies on friction dampers were conducted [1–6]. Recently, Samani et al. have studied on hysteretic behaviour of a cylindrical frictional device under dynamic loading [7]. Mirzabagheri et al. have reported experimental and numerical investigation of rotational friction devices with multiunits [8]. Wu et al. have conducted an experimental study on reparability of an infilled rocking wall frame structure with rotational and translational friction devices [9]. Tsampras et al. have experimentally investigated on deformable connection consisted of a friction device [10].

In general, passive vibration control systems have optimal damper characteristics, such as the slip force of friction

dampers, which can minimize seismic responses. Inoue and Kuwahara studied on an optimal strength ratio of hysteretic dampers based on equivalent damping [11]. Shirai et al. investigated an optimal yield strength ratio of elastic-plastic damper based on transfer function of the equivalent linear system [12, 13]. Recently, Ontiveros-Pérez et al. have assessed a simultaneous optimization of friction dampers [14]. Qu and Li have studied on optimal placement and reasonable number of viscoelastic dampers [15]. Mirzaeefard and Mirtaheri have investigated the seismic behaviour of a steel structure model incorporating cylindrical frictional dampers and the optimal slip load characteristics of the friction-damped system [16]. As for friction devices that can produce various magnitudes of the slip force, Samani et al. have reported a study on a semiactive frictional device with various control algorithms [17].

It is useful to determine the optimal damper characteristics in the design of vibration control structures for earthquakes. However, the optimal damper characteristics

vary depending on various factors as reported by Shirai et al. [12, 13]. Although it is recognized that sway-rocking motion under structures affects the earthquake response of superstructures, a limited number of analytical and theoretical studies have investigated the optimal or effective damper characteristics of vibration control systems considering sway-rocking motion. Takewaki studied on effective damper placement for shear-flexural building structure models with soil-structure interaction [18]. Tsuruga and Motosaka investigated on optimal damper placement considering soil-structure interaction [19]. Recently, Koya et al. have assessed optimal damping characteristics of vibration control systems with Maxwell-type or hysteretic damper in consideration of sway-rocking motion [20, 21]. Zhao et al. have investigated on the optimal design of viscoelastic dampers in frame structures considering soil-structure interaction [22]. In addition, since very few experimental studies have been conducted, more studies especially based on experimental data are therefore needed to clarify the optimal damper characteristics of the passive control systems with sway-rocking motion.

The objective of the present study is to experimentally determine the optimal slip force of friction-damped structures with sway-rocking motion. A series of shaking table tests were carried out using a specimen composed of a vibration control superstructure and a sway-rocking mechanism under the superstructure. Efficiently conducting many shaking table tests and obtaining the corresponding responses under various conditions, such as various magnitudes of the friction damper force, were considered in the planning of the tests and specimen in order to obtain the optimal damper slip force for the vibration control system. A friction device that allowed the magnitude of the slip force to be easily set was adopted for the superstructure. For the lower structure, it was necessary to carry out a large number of tests with various magnitudes of the slip force of the friction device, with the other conditions fixed. The sway-rocking mechanism thus consisted of mechanical elements with high reproducibility.

In addition, this study expands upon previous studies [23–25] by presenting new experimental results and findings. In the present paper, Shirai and Fujimori designed the study and experiments. Nagaoka and Shirai performed the experiments. Nagaoka, Fujita, and Shirai analysed the data. Shirai wrote the paper with input from all authors.

2. Test Specimen

2.1. Main Frame and Sway-Rocking Mechanism. The test specimen was designed and manufactured for use in shaking table tests. Figure 1 shows a photograph of the front of the specimen. Figures 2 and 3 show the plan and elevation drawings of the specimen, respectively. The specimen was composed of the vibration control superstructure model incorporating the friction device, and the sway-rocking mechanism was placed under the superstructure. The main frame of the superstructure consisted of four stainless steel plates acting as columns and a rigid beam on the top of these plates.

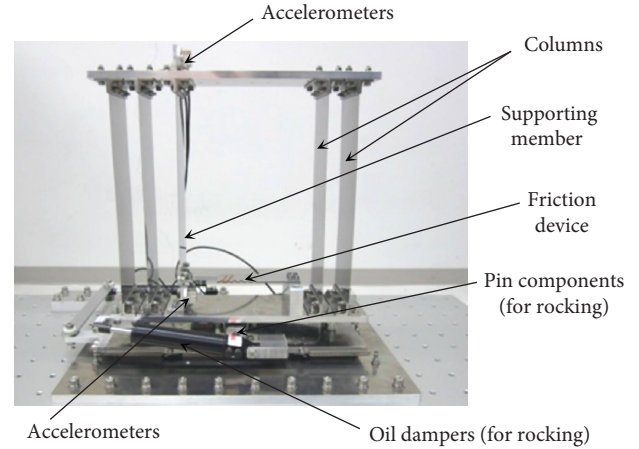


FIGURE 1: Front view of specimen.

Figure 4 shows a photograph of the front of the sway-rocking mechanism. For the sway part, linear guides (SRS12M) as horizontal bearings and horizontal tensile coil springs as restoring force members were installed into the sway story above the shaking table. For the rocking part, pin components as a centre of rotation and compression coil springs as vertical restoring force members were placed above the sway part. To dampen the sway and rocking motions, one and two small oil dampers (ADA505M) were installed, respectively, into the sway and rocking parts. Since the viscous damping coefficient of each oil damper, c_d , was too large to use directly, the viscous damping for the sway and rocking parts was adjusted as follows.

For the sway part, the horizontal viscous damping coefficient, c_{sw} , was decreased by adopting the principle of leverage, as shown in equation (1), such that c_{sw} agreed with the target viscous damping coefficient in the horizontal direction:

$$c_{sw} = \frac{c_d}{\alpha^2}, \quad (1)$$

where α is the lever magnification and c_d is the viscous damping coefficient of the oil damper. One oil damper was installed with a lever such that $\alpha = 14.1$ for the sway part (Figure 2).

For the rocking part, the rotational viscous damping coefficient, c_{ro} , was decreased by inclining the mounting angles of the oil dampers, as shown in equation (2), such that c_{ro} agreed with the target viscous damping coefficient in the rotational direction:

$$c_{ro}\omega = 2(c_d \cos^2 \theta)r^2\omega, \quad (2)$$

where ω is the angular velocity, c_d is the viscous damping coefficient of each oil damper, r is the radius of gyration, and θ is the mounting angle of each oil damper. Two oil dampers were installed with mounting angles of $\theta = 81.7^\circ$ (Figures 2 and 3).

The specifications of the specimen are shown in Table 1. In this table, Method 1 is the direct measurement, Method 2 is calculation based on the sizes of the members and catalogue specifications, Method 3 is calculation based on

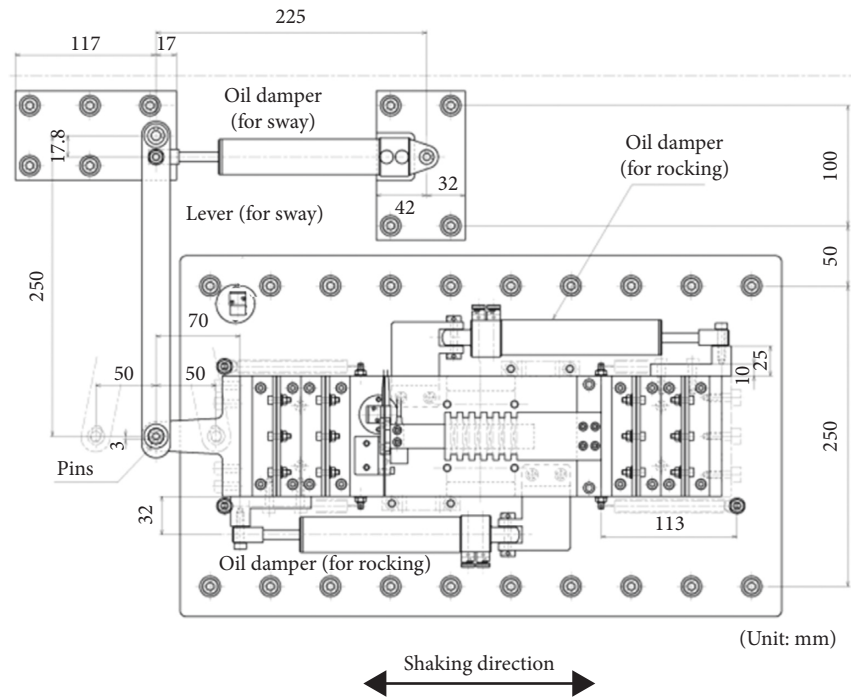


FIGURE 2: Plan view of specimen.

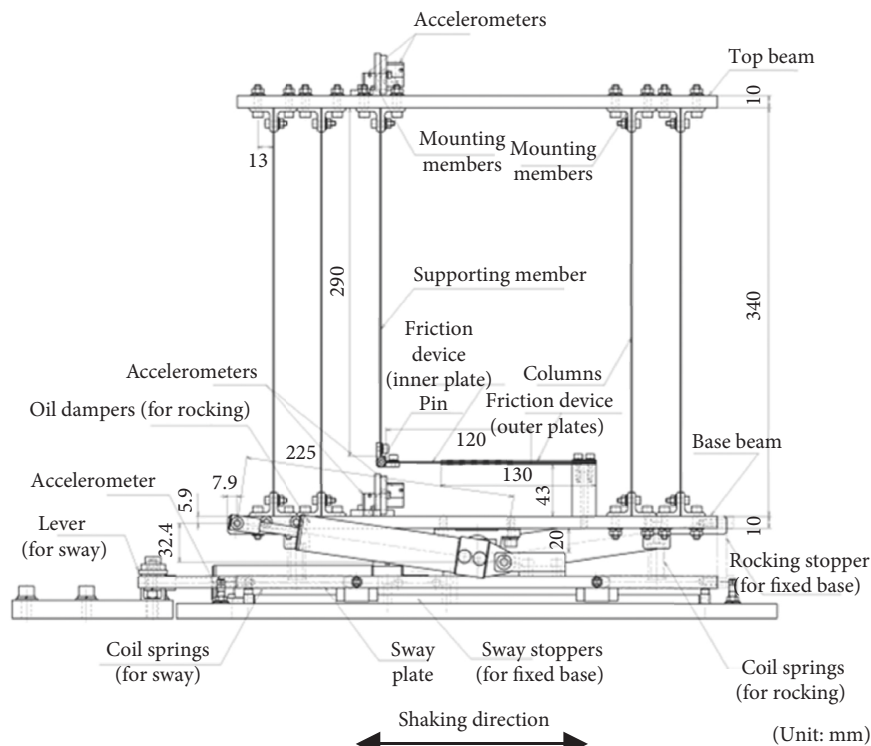


FIGURE 3: Elevation view of specimen.

natural periods obtained in free vibration tests (Section 3.1), Method 4 is the preliminary static measurement using spring balances (Section 2.3), and Method 5 is evaluation of the slip force based on response hysteresis loops using shaking table tests (Section 4.2).

2.2. Specimen Design. The specimen was modelled based on a design example of a full-scale building, in which sway-rocking motion due to soil-structure interaction was taken into account [26]. The full-scale building was a six-story reinforced concrete and beam-column frame structure with a pile foundation.

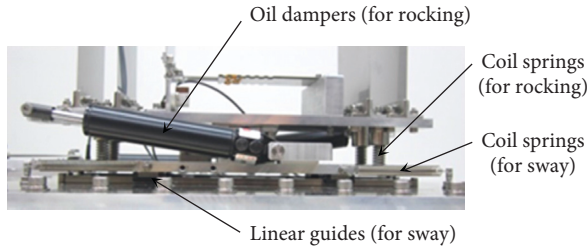


FIGURE 4: Front view of sway-rocking mechanism.

TABLE 1: Specifications of specimen.

Property	Component	Method	Value
Slip force	Friction device	4 and 5	Parameter
Height (top to pin component)	Main frame	1	0.39 m
Horizontal stiffness	Main frame	3	1.48 N/cm
Mass (upper half)	Main frame	1	2.58 kg
Moment of inertia (upper half)	Main frame	2	344 kg·cm ²
Mass	Base	1	5.56 kg
Moment of inertia	Base	2	482 kg·cm ²
Horizontal stiffness	Sway part	2	4.92 N/cm
Horizontal damping coefficient	Sway part	2	0.224 Ns/cm
Rotational stiffness	Rocking part	3	4.10 × 10 ⁴ N·cm/rad
Rotational damping coefficient	Rocking part	2	740 Ns·cm/rad

Properties of the superstructure and the sway-rocking springs of the full-scale building are given in Tables 2 and 3, respectively [26]. In Table 2, K_1 is the initial stiffness, K_2 is the tangent stiffness between crack and yield points, K_3 is the tangent stiffness after yield point, Q_1 is the shear force at the crack point, and Q_2 is the shear force at the yield point for each story of the superstructure.

The specimen was designed for each type of sway and rocking condition (fixed base, sway, rocking, and sway-rocking) such that the natural period ratio and damping factor of the specimen (without a friction device) obtained from complex eigenvalue analysis were approximately equal to those of the full-scale building, the stiffness of which was the secant stiffness at its yield point.

Table 4 shows the natural period ratios and damping factors obtained from the complex eigenvalue analysis. In this table, T_{FI} , T_{SW} , T_{RO} , and T_{SR} are the natural periods for fixed base, under sway motion, under rocking motion, and under sway-rocking motion, respectively. Moreover, h_{SW} , h_{RO} , and h_{SR} are the damping factors under sway motion, under rocking motion, and under sway-rocking motion, respectively.

Considering the similarity rule for the design of the specimen, the time axis of each input motion used in the shaking table tests was adjusted as described in Section 3.2.2.

2.3. Friction Device. In this study, to experimentally obtain the optimal damper slip force, a simple friction device was

adopted. Figure 5 shows a photograph of the friction device. This device was composed of rubber bands and stainless steel plates. The device allowed the magnitude of the slip force to be easily set by changing the configuration of the rubber bands, as shown in Figures 6(a)–6(d). The optimal damper slip force, which most effectively minimizes the earthquake response, was determined using the friction device. A supporting member made of a stainless steel plate (thickness: 1.0 mm) was connected in series to the friction device. The friction device and the supporting member were incorporated into the main story of the superstructure.

In this study, before the shaking table tests, the slip forces for various rubber band configurations of the friction device as shown in Figures 6(a)–6(d) were obtained by conducting a preliminary measurement via static pull tests on the friction device alone using spring balances, as depicted in Figure 6(e). Hereafter, the slip force obtained from the preliminary measurement using spring balances is denoted as F_D .

3. Test Methods

3.1. Free Vibration Tests. Prior to the shaking table tests, free vibration tests were conducted under each type of sway and rocking condition (both sway and rocking fixed; sway fixed and rocking movable; sway not fixed and rocking fixed; and sway not fixed and rocking movable) and friction device condition (device fixed or not device). The natural periods and damping factors obtained from the free vibration tests are shown in Table 5. From the results, the ratio of the horizontal stiffness of the supporting member connected in series to the friction device to that of the main frame of the superstructure was calculated as $K_B/K_F = 1.50$.

3.2. Shaking Table Tests

3.2.1. Measurement Procedure and Shaking Table. In this study, the response absolute accelerations were measured using strain-type accelerometers attached to typical parts of the specimen and the shaking table (i.e., the top of the superstructure, the top of the sway-rocking mechanism, and the top of the shaking table). The response displacements were obtained by doubly integrating the response acceleration data.

For the shaking table tests, a unidirectional shaking table was used with a maximum payload of 1000 N, a maximum excitation acceleration of 1.0 G, and a size of 1000 mm × 500 mm.

3.2.2. Input Earthquake Motions. As input ground motions, five simulated earthquake waves, namely, Waves L1 through L5, were used in this study. Examples of the response velocity spectra observed on the shaking table during the tests are shown in Figure 7 for Wave L1 with various input levels (×0.2, ×0.3, and ×0.4). These five waves were fitted to the target response acceleration spectrum provided by Notification No. 1461 of the Ministry of Construction in 2000 (in accordance with the Building Standard Law Enforcement

TABLE 2: Properties of superstructure of full-scale building [26].

Floor	Height (m)	Weight (kN)	K_1 (kN/m)	K_2 (kN/m)	K_3 (kN/m)	Q_1 (kN)	Q_2 (kN)
6	2.85	4681	2.22×10^6	3.13×10^5	2.50×10^3	1567	3536
5	2.85	4902	2.42×10^6	3.50×10^5	1.27×10^4	2403	5598
4	2.85	4902	2.47×10^6	4.07×10^5	3.19×10^4	2819	6949
3	2.85	5096	2.58×10^6	4.77×10^5	4.44×10^4	3319	8239
2	2.85	5096	2.36×10^6	4.83×10^5	5.06×10^4	4530	9514
1	3.45	5100	3.05×10^6	5.10×10^5	3.50×10^4	5062	11383
Base	—	7792*	—	—	—	—	—

* Moment of inertia: $8.14 \times 10^5 \text{ kNm}^2$.

TABLE 3: Properties of sway-rocking springs of full-scale building [26].

Component	Property	Value
Sway	Stiffness	$6.10 \times 10^5 \text{ kN/m}$
Sway	Damping coefficient	$2.69 \times 10^4 \text{ kN}\cdot\text{s/m}$
Rocking	Stiffness	$1.88 \times 10^9 \text{ kN}\cdot\text{m/rad}$
Rocking	Damping coefficient	$1.18 \times 10^7 \text{ kN}\cdot\text{ms/rad}$

TABLE 4: Natural period ratios and damping factors obtained from complex eigenvalue analysis.

Natural period ratio/damping factor	Full-scale building ¹	Specimen ²
T_{SW}/T_{FI}	1.19	1.24
T_{RO}/T_{FI}	1.01	1.03
T_{SR}/T_{FI}	1.19	1.25
h_{SW}	5.14%	6.57%
h_{RO}	0.05%	0.35%
h_{SR}	5.06%	6.30%

¹Corresponds to secant stiffness at the yielding point for each story of the main frame of the superstructure. ²Calculated from sizes of members and catalogue specifications (without the friction device, not considering resistance force of linear guides at the sway part).

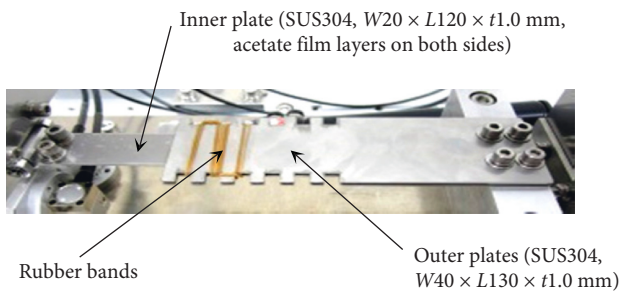


FIGURE 5: Friction device.

Order of Japan) [27]. Considering the capacity of the shaking table, components exceeding a period of 2.0 s were cut off in the frequency domain for each input motion. The time axis of each wave was adjusted such that the ratio of the corner period of the target response spectrum to the natural period of the specimen agreed with that of the full-scale building. The time-domain envelope functions proposed by Amin and Ang [28] were used. The duration of the steady part of each wave was set to be 42 s. Random values were used for the phase angles of each wave.

3.2.3. Test Parameters. The main test parameter was the slip force of the friction device (approximately 13 levels; e.g., small, moderate, and excessive force). The other test parameters were the input level (i.e., multiplying factors of the input motions of $\times 0.2$, $\times 0.3$, and $\times 0.4$), sway-rocking condition (fixed base and sway-rocking), and input wave (Waves L1 through L5). As a result, over 370 shaking table tests were conducted.

4. Results of Shaking Table Tests

4.1. Response Behaviour. Figures 8 and 9 show examples of the time history acceleration response in the horizontal direction measured by accelerometers placed at the typical points (i.e., top of the shaking table, top of the sway-rocking mechanism, and top of the superstructure) for input levels of $\times 0.3$ and $\times 0.4$ (sway-rocking, Wave L1), respectively.

Figures 10 and 11 show examples of response hysteresis loops for the main frame of the superstructure and the sway story in the horizontal direction for input levels of $\times 0.3$ and $\times 0.4$ (sway-rocking, Wave L1), respectively. In these figures, the horizontal axis is the relative story drift and the vertical axis is the story shear force (calculated from the inertial force). Figures 10(a) and 11(a) depict the hysteresis loops of the superstructure for small slip forces of the friction device. Figures 10(b) and 11(b) show the responses of the superstructure for moderate slip forces. From these figures, the friction device adopted in this study exhibited approximately bilinear hysteresis loops. Figures 10(c) and 11(c) show the hysteresis loops of the superstructure for slip forces larger than the optimal damper forces. Figures 10(d) and 11(d) depict the response hysteresis loops of the sway story, showing a combination of ellipse behaviour, due to the oil damper for the sway part, and bilinear behaviour, due to the resistance force of the linear guides installed in the sway part.

4.2. Evaluation of Slip Force of Friction Device Based on Response Hysteresis Loops. In order to investigate the optimal damper characteristics using a more accurate slip force of the friction device, evaluation of the slip force based on the response hysteresis loops obtained from the shaking table tests was conducted. Figure 12 shows conceptual diagrams of the slip force evaluation. First, by subtracting the secondary stiffness corresponding to the main frame stiffness from the hysteresis loops of the superstructure, as shown in Figure 12(a), the hysteresis loops of the friction device force were obtained, as shown in Figure 12(b). Then, the hysteresis

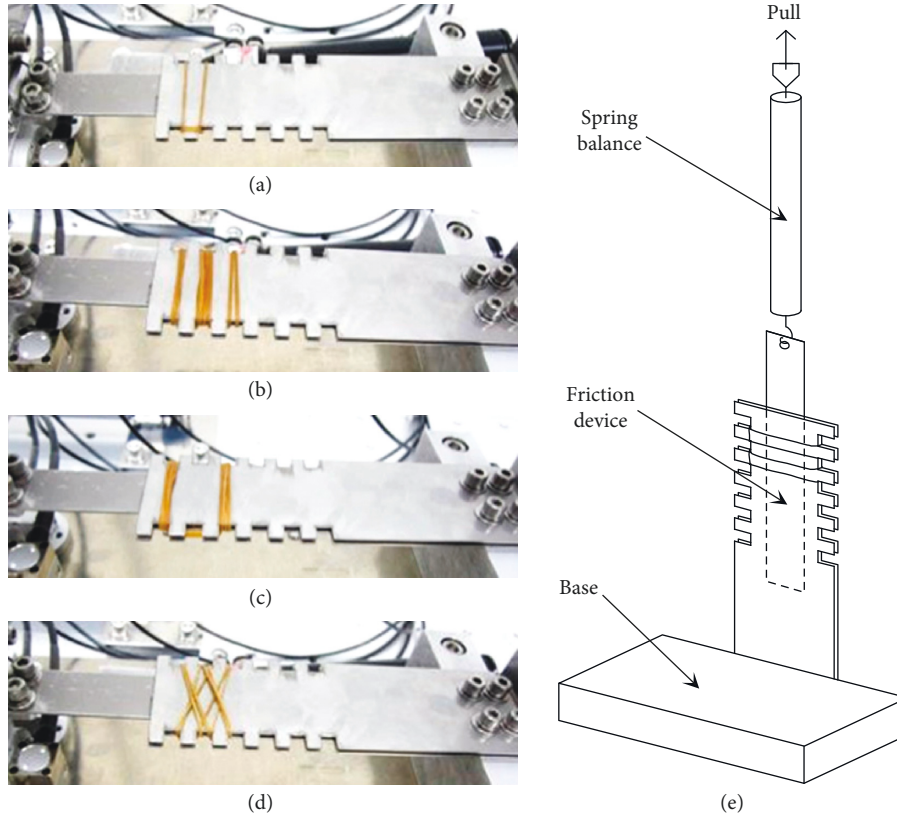


FIGURE 6: Slip force of friction device. Examples of rubber band configurations: (a) $F_D = 0.35$ N; (b) $F_D = 1.65$ N; (c) $F_D = 2.0$ N; (d) $F_D = 2.25$ N. (e) Diagram of preliminary measurement using spring balance.

TABLE 5: Results of free vibration tests.

Sway-rocking motion		Friction device condition	Natural period (s)	Damping factor (%)
Sway	Rocking			
Fixed	Fixed	Fixed	0.52	0.26
Fixed	Fixed	No device	0.83	0.27
Fixed	Movable	No device	0.85	0.31
Not fixed ¹	Fixed	No device	0.88	0.25
Not fixed ¹	Movable	No device	0.91	0.31

¹Sway part did not move due to resistance force of linear guides.

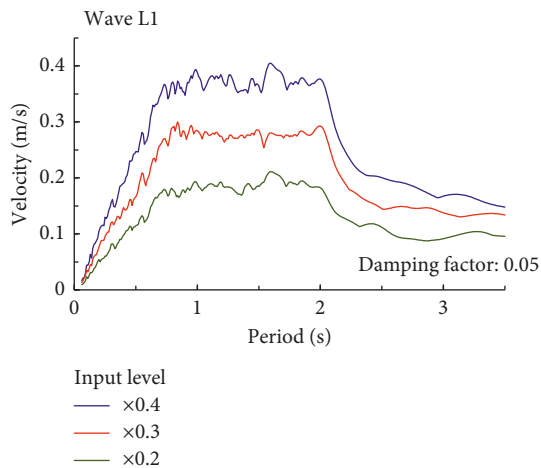


FIGURE 7: Velocity response spectra of input motions.

loops at the peak story drift were classified into several cases according to their shapes. For the typical case, an equivalent slip force in terms of the energy absorption was obtained based on the area of the half-cycle loop, including the peak story drift point on the negative side, as shown in Figure 12(b) with the bold line. Hereafter, the average value of the three waves, excluding the maximum and minimum values, among the evaluated equivalent slip forces for the five input motions (Waves L1 through L5) obtained using the above method is adopted; it is denoted F'_D .

Figure 13 compares the evaluated equivalent slip force based on the response hysteresis loops (F'_D) and the slip force obtained from the preliminary measurement using spring balances described in Section 2.3 (F_D). F'_D tends to produce a slip force that is approximately the same as or slightly larger than F_D . In the following sections, F'_D is used for determining the optimal damper slip force.

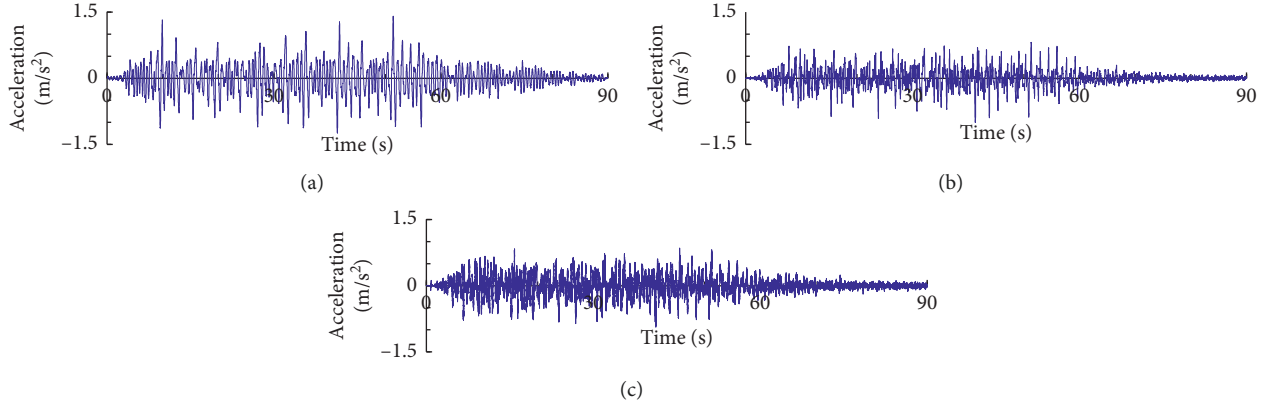


FIGURE 8: Response time history accelerations for input level of $\times 0.3$. (a) Top of superstructure, (b) top of sway-rocking mechanism, and (c) shaking table.

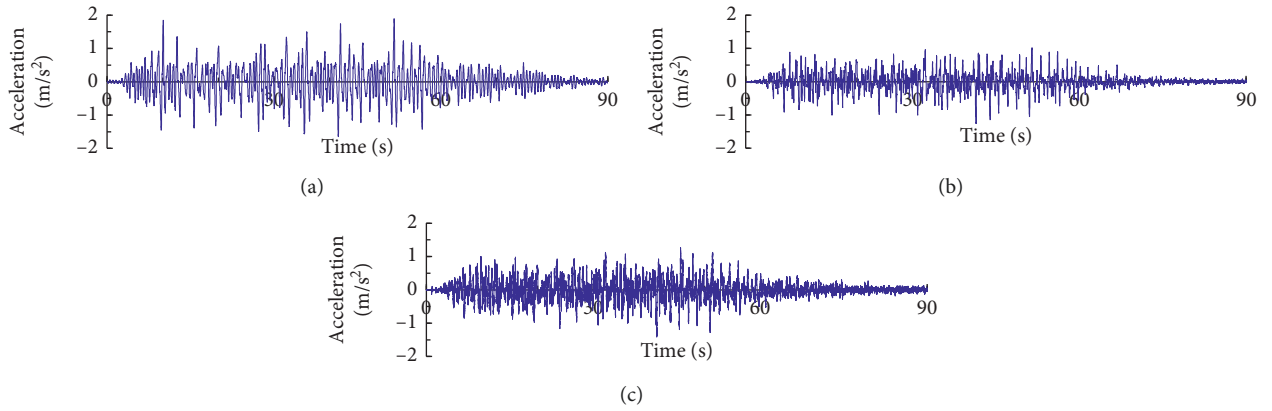


FIGURE 9: Response time history accelerations for input level of $\times 0.4$. (a) Top of superstructure, (b) top of sway-rocking mechanism, and (c) shaking table.

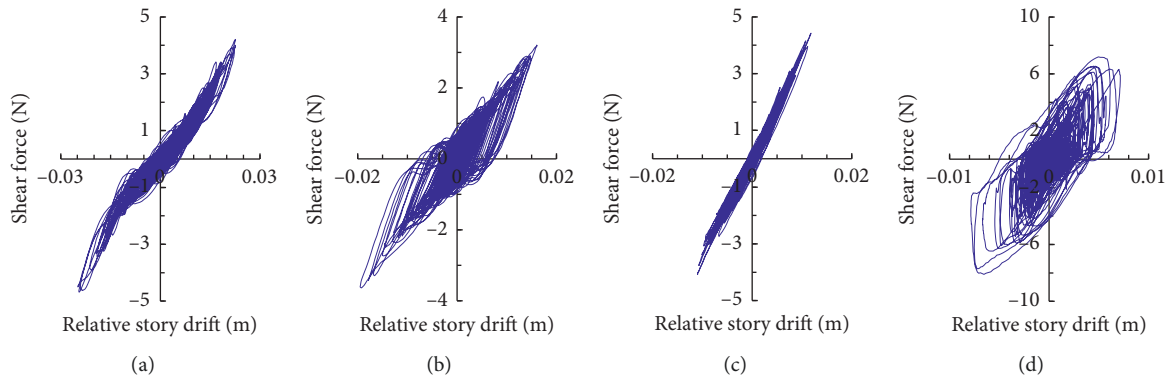


FIGURE 10: Hysteresis loops for input level of $\times 0.3$. Superstructure: (a) $F_D = 0.1$ N; (b) $F_D = 0.55$ N; (c) $F_D = 3.1$ N. Sway story. (d) $F_D = 0.1$ N.

4.3. Optimal Damper Slip Force for Minimizing Peak Response.

Figures 14 and 15 show the relationships between the peak response and the evaluated equivalent slip force, F'_D , for each input level for fixed base and under sway-rocking motion, respectively. For Figures 14(a) and 15(a), the vertical axis is the peak acceleration at the top of the superstructure. For Figures 14(b) and 15(b), the vertical axis is the peak relative story drift of the superstructure. In Figures 14 and 15, each

solid or dashed line represents the response curve of the mean of the peak responses of the five input motions (Waves L1 through L5). From these figures, the existence of an optimal slip force of the friction device that minimizes the response curve of the peak response was experimentally confirmed for each condition. Moreover, the obtained response curves under sway-rocking motion exhibited gentler changes with increasing F'_D compared with those for the fixed base.

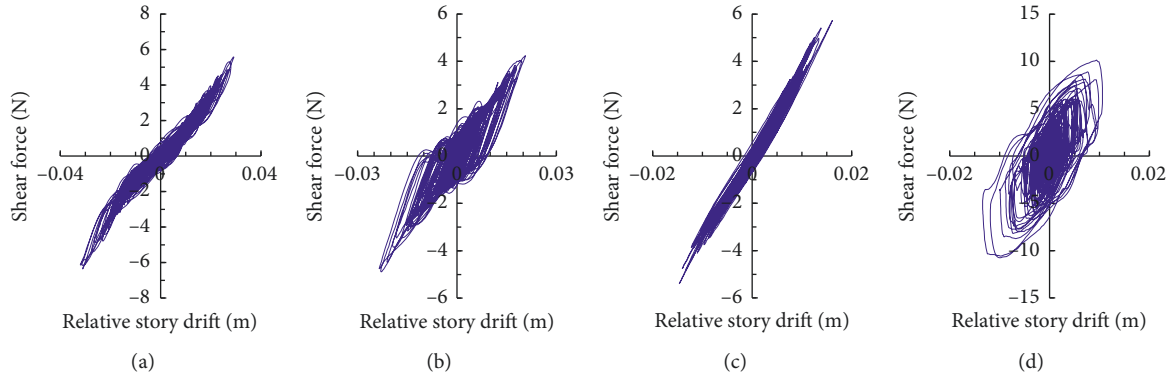


FIGURE 11: Hysteresis loops for input level of $\times 0.4$. Superstructure: (a) $F_D = 0.1$ N; (b) $F_D = 0.75$ N; (c) $F_D = 3.1$ N. Sway story: (d) $F_D = 0.1$ N.

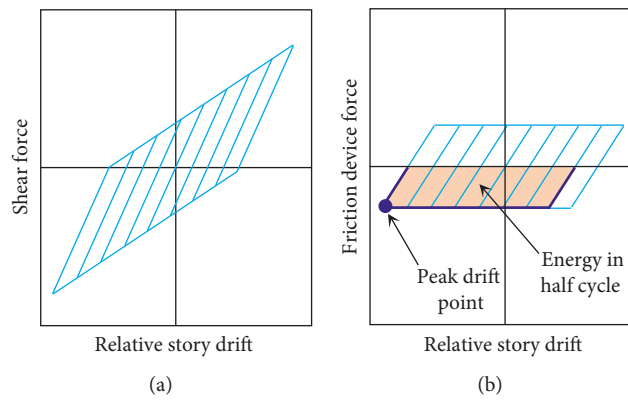


FIGURE 12: Conceptual diagrams of evaluation of slip force of the friction device based on response hysteresis loops of superstructure. Hysteresis loops of (a) superstructure and (b) friction device force.

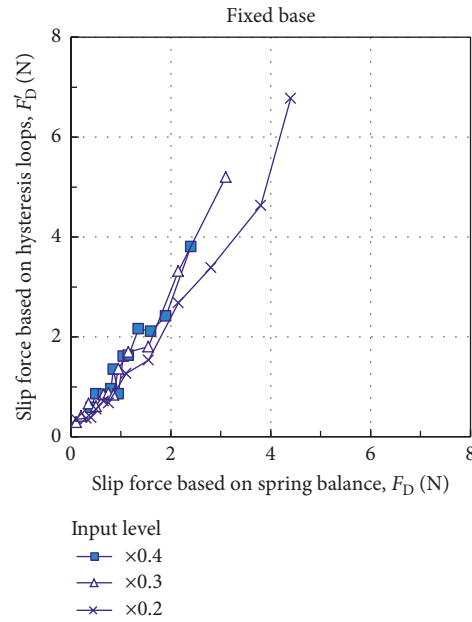


FIGURE 13: Comparison of slip force of the friction device based on spring balance measurement, F_D , and that based on hysteresis loops, F'_D .

Figure 16 compares the optimal slip force of the friction device that minimized the response curve of the peak response for each input level and each sway-rocking condition.

In this figure, $F'_{D,opt,Acc}$ and $F'_{D,opt,Disp}$ denote the optimal slip forces for minimizing the response curve of the peak response acceleration and the peak response story drift,

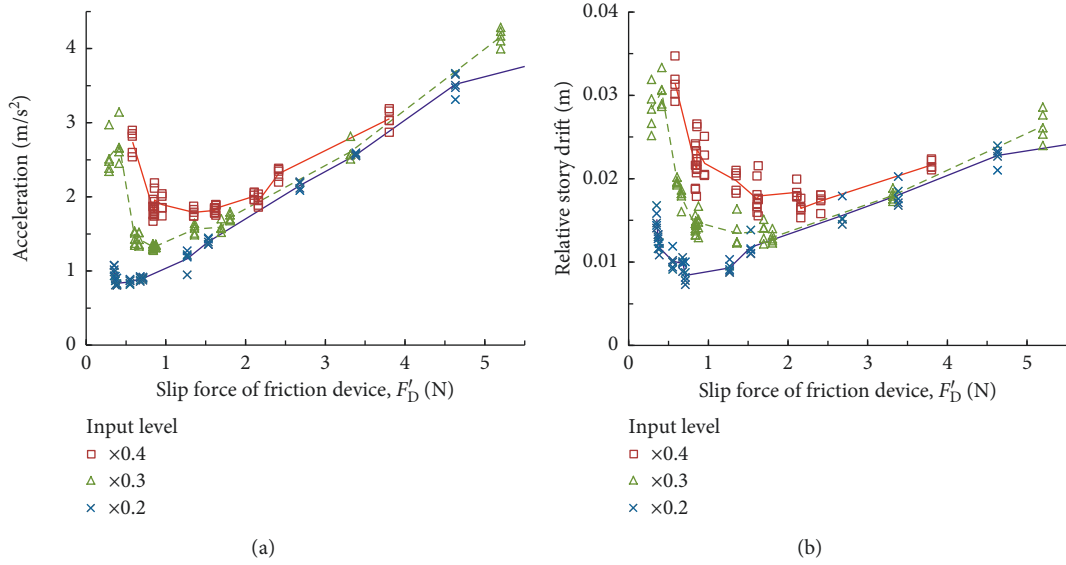


FIGURE 14: Relationships between peak response and F'_D for fixed base. Response curves of (a) peak acceleration at top of superstructure and (b) peak relative story drift of main frame of superstructure.

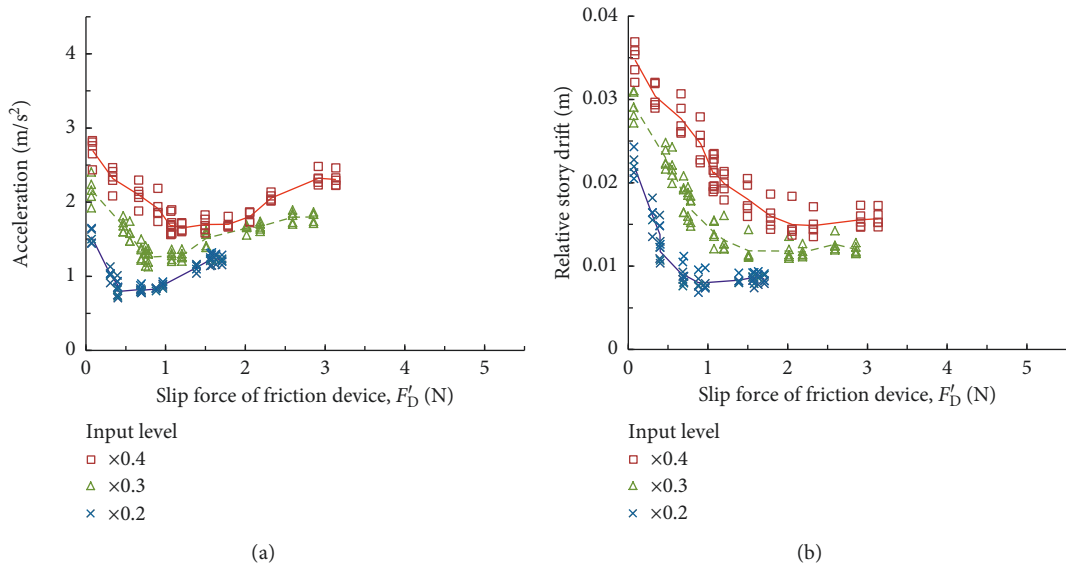


FIGURE 15: Relationships between peak response and F'_D under sway-rocking. Response curves of (a) peak acceleration at top of superstructure and (b) peak relative story drift of main frame of superstructure.

respectively. From this figure, as the input level increased, the optimal slip forces ($F'_{D,\text{opt,Acc}}$ and $F'_{D,\text{opt,Disp}}$) increased. Moreover, $F'_{D,\text{opt,Disp}}$ was larger than $F'_{D,\text{opt,Acc}}$.

4.4. Optimal Damper Slip Force for Minimizing Root-Mean-Square Response. The root-mean-square (RMS) response is closely related to the peak response of structures subjected to earthquakes [29]. In the present study, the RMS acceleration at the top of the superstructure was obtained as follows:

$$\text{RMS acceleration} = \sqrt{\frac{1}{t_d} \int_{t_1}^{t_2} |x_{\text{Acc}}(t)|^2 dt}, \quad (3)$$

where t is the time, $x_{\text{Acc}}(t)$ is the time history response acceleration at the top of the superstructure in the horizontal direction, t_d is the duration of the input motion, t_1 is the starting time of t_d , and t_2 is the ending time of t_d . In the present study, t_d was calculated according to the definition of the time interval during which the central 90% of the contribution to the integral of the square of input acceleration takes place [29, 30].

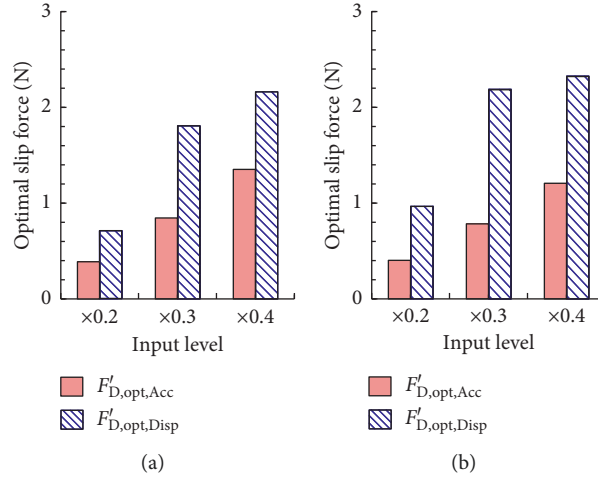


FIGURE 16: Comparison of optimal slip force of the friction device that minimizes peak response curve for (a) fixed base and (b) sway-rocking.

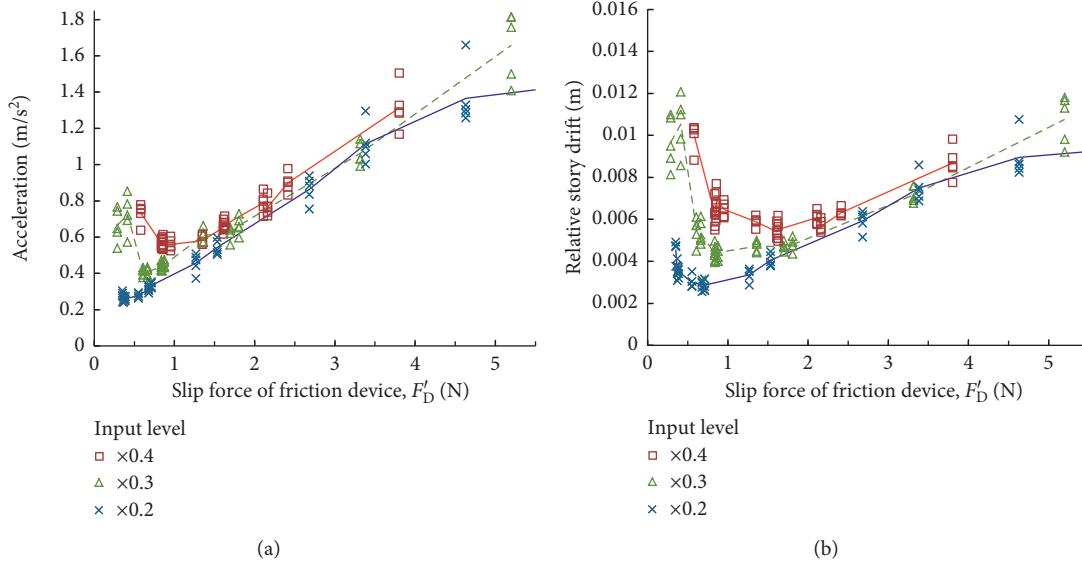


FIGURE 17: Relationships between RMS response and F'_D for fixed base. Response curves of (a) RMS acceleration at top of superstructure and (b) RMS relative story drift of main frame of superstructure.

The RMS relative story drift of the superstructure was obtained as follows:

$$\text{RMS relative story drift} = \sqrt{\frac{1}{t_2 - t_1} \int_{t_1}^{t_2} |x_{\text{Disp}}(t)|^2 dt}, \quad (4)$$

where $x_{\text{Disp}}(t)$ is the time history response relative story drift of the superstructure in the horizontal direction.

The relationships between the RMS response and F'_D are shown in Figures 17 and 18. For Figures 17(a) and 18(a), the vertical axis is the RMS acceleration at the top of the superstructure. For Figures 17(b) and 18(b), the vertical axis is the RMS relative story drift of the superstructure. The obtained response curve, i.e., the mean of the RMS response for the five waves, depicted by the solid or dashed line, indicates the existence of an optimal slip force for each condition. In

addition, the RMS response curves under sway-rocking motion showed gentler changes compared with those for the fixed base.

The optimal slip forces of the friction device ($F'_{D,opt,Acc}$ and $F'_{D,opt,Disp}$) that minimized the response curve for RMS acceleration on the top of the superstructure and the relative story drift of the superstructure are compared in Figure 19. From this figure, a tendency similar to that of the peak response (Figure 16) was found for the optimal slip force that minimizes the RMS response. In addition, the optimal slip forces ($F'_{D,opt,Acc}$ and $F'_{D,opt,Disp}$) under sway-rocking motion were slightly larger than that for the fixed base.

The results obtained in Sections 4.3 and 4.4 show that the optimal damper slip force for minimizing the peak and RMS responses varies depending on the input level of the ground motions and the sway-rocking conditions.

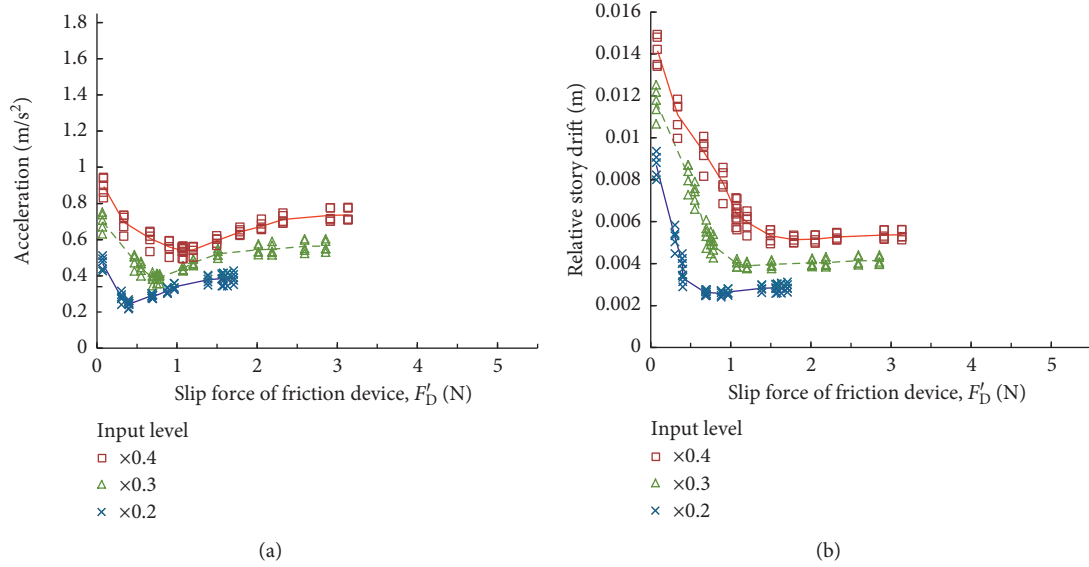


FIGURE 18: Relationships between RMS response and F'_D under sway-rocking. Response curves of (a) RMS acceleration at top of superstructure and (b) RMS relative story drift of main frame of superstructure.

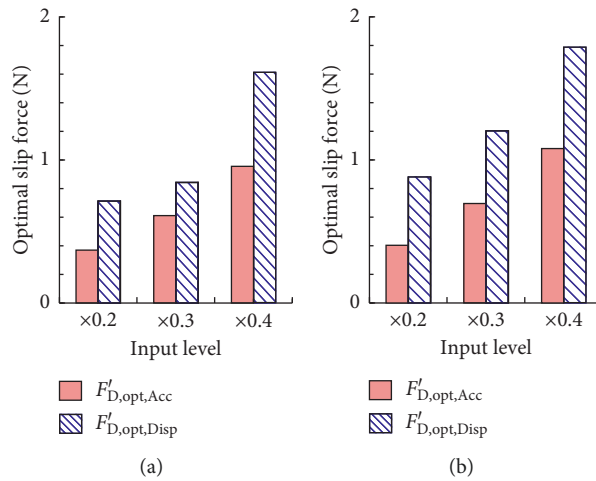


FIGURE 19: Comparison of optimal slip force of the friction device that minimizes RMS response curve for (a) fixed base and (b) sway-rocking.

5. Conclusions

In this study, a series of shaking table tests were conducted using a superstructure incorporating a friction device with a sway-rocking mechanism for determining the optimal damper slip force of a passive vibration control system for fixed base and sway-rocking motion. From the results, the following conclusions can be drawn:

- (1) For the shaking table tests, a simple friction device that allowed the magnitude of the slip force to be easily set was used to determine the optimal damper slip force that effectively minimized the peak and RMS responses.
- (2) The results of the shaking table tests demonstrate that the optimal slip force of the friction device for minimizing the peak and RMS responses

of the superstructure varies depending on the input level of the earthquakes and sway-rocking conditions.

- (3) For peak and RMS responses, as the input level increased, the optimal slip force increased. In addition, the optimal slip force for relative story drift was larger compared to that for acceleration. The optimal slip force that minimizes the RMS response under sway-rocking motion was slightly larger than that for fixed base.
- (4) The results suggest that the effect of sway-rocking motion should be considered in the design of passive vibration control systems and the determination of their optimal damper slip force.
- (5) The findings obtained in this study will contribute to the optimal design of vibration control systems

considering soil-structure interaction. Furthermore, the test methods used in this study can be used as a basis for conducting further experimental research in the future on friction-damped structures considering soil-structure interaction. The sway-rocking mechanism of the specimen can be improved to better reflect actual conditions.

For future challenge, analytical studies using more realistic building and soil models are needed for establishing the optimal design method for passive control structures considering soil-structure interaction. In that case, the evaluation method for the optimal slip force of friction damped systems such as adopted in reference [16] may be one of the helpful approaches.

Data Availability

Requests for the data used to support the findings of this study will be considered by the corresponding author.

Conflicts of Interest

The authors declare that there are no conflicts of interest regarding the publication of this paper.

Acknowledgments

This study was supported by JSPS KAKENHI (Grant numbers JP 24760441 and JP 16K06564), and a 2013 research grant from the Toda Scholarship Foundation.

References

- [1] A. S. Pall and C. Marsh, "Response of friction damped braced frames," *Journal of the Structural Division (ASCE)*, vol. 108, no. 6, pp. 1313–1323, 1982.
- [2] K. Roik, U. Dorka, and P. Dechent, "Vibration control of structures under earthquake loading by three-stage friction-grip elements," *Earthquake Engineering & Structural Dynamics*, vol. 16, no. 4, pp. 501–521, 1988.
- [3] T. F. FitzGerald, T. Anagnos, M. Goodson, and T. Zsutty, "Slotted bolted connections in aseismic design for concentrically braced connections," *Earthquake Spectra*, vol. 5, no. 2, pp. 383–391, 1989.
- [4] Y. Takahashi and Y. Suzui, "Development of friction slip dampers using high-tension bolts: part 1," in *Proceedings of Summaries of Technical Papers of Annual Meeting*, Architectural Institute of Japan, pp. 979–980 Tokyo, Japan, September 2000, in Japanese.
- [5] I. H. Mualla and B. Belev, "Performance of steel frames with a new friction damper device under earthquake excitation," *Engineering Structures*, vol. 24, no. 3, pp. 365–371, 2002.
- [6] T. Sano and H. Katsumata, "Development of advanced friction sliding damper," in *Proceedings of 14th World Conference on Earthquake Engineering*, Beijing, China, October 2008.
- [7] H. R. Samani, M. Mirtaheri, A. P. Zandi, and H. Bahai, "The effects of dynamic loading on hysteretic behavior of frictional dampers," *Shock and Vibration*, vol. 2014, Article ID 181534, 9 pages, 2014.
- [8] S. Mirzabagheri, M. Sanati, A. A. Aghakouchak, and S. E. Khadem, "Experimental and numerical investigation of rotational friction dampers with multi units in steel frames subjected to lateral excitation," *Archives of Civil and Mechanical Engineering*, vol. 15, no. 2, pp. 479–491, 2015.
- [9] S. Wu, P. Pan, X. Nie, H. Wang, and S. Shen, "Experimental investigation on reparability of an infilled rocking wall frame structure," *Earthquake Engineering & Structural Dynamics*, vol. 46, no. 15, pp. 2777–2792, 2017.
- [10] G. Tsampras, R. Sause, R. B. Fleischman, and J. I. Restrepo, "Experimental study of deformable connection consisting of friction device and rubber bearings to connect floor system to lateral force resisting system," *Earthquake Engineering & Structural Dynamics*, vol. 47, no. 4, pp. 1032–1053, 2017.
- [11] K. Inoue and S. Kuwahara, "Optimum strength ratio of hysteretic damper," *Earthquake Engineering & Structural Dynamics*, vol. 27, no. 6, pp. 577–588, 1998.
- [12] K. Shirai, M. Kageyama, K. Ikago, and N. Inoue, "Study on optimum damper yield strength based on transfer function of equivalent linear system for R/C structure with hysteretic damper," *Journal of Structural and Construction Engineering (Transactions of AIJ)*, vol. 76, no. 666, pp. 1433–1442, 2011, in Japanese.
- [13] K. Shirai, M. Kageyama, K. Ikago, and N. Inoue, "Optimum yield strength of a hysteretic damper incorporated into RC structures using the transfer function of an equivalent linear system," in *Proceedings of 13th World Conference on Seismic Isolation, Energy Dissipation and Active Vibration Control of Structures*, vol. 120, pp. 1–8, Sendai, Japan, September 2013.
- [14] S. P. Ontiveros-Pérez, L. F. F. Miguel, and L. F. F. Miguel, "A new assessment in the simultaneous optimization of friction dampers in plane and spatial civil structures," *Mathematical Problems in Engineering*, vol. 2017, Article ID 6040986, 18 pages, 2017.
- [15] J.-t. Qu and H.-n. Li, "Study on optimal placement and reasonable number of viscoelastic dampers by improved weight coefficient method," *Mathematical Problems in Engineering*, vol. 2013, Article ID 358709, 10 pages, 2013.
- [16] H. Mirzaeefard and M. Mirtaheri, "Seismic behavior of steel structures equipped with cylindrical frictional dampers," *Asian Journal of Civil Engineering (BHRC)*, vol. 17, no. 5, pp. 651–661, 2016.
- [17] H. R. Samani, M. Mirtaheri, and A. P. Zandi, "The study of frictional damper with various control algorithms," *Earthquakes and Structures*, vol. 12, no. 5, pp. 479–487, 2017.
- [18] I. Takewaki, "Seismically effective damper placement for shear-flexural building models including soil structure interaction," *Journal of Structural and Construction Engineering (Transactions of AIJ)*, vol. 65, no. 530, pp. 77–84, 2000, in Japanese.
- [19] T. Tsuruga and M. Motosaka, "Optimal damper placement for soil-structure interaction system," *Research Reports of AIJ Tohoku Branch*, vol. 63, pp. 149–152, 2000, in Japanese.
- [20] T. Koya, K. Shirai, T. Fujimori, and M. Kikuchi, "Optimum damping characteristic evaluation of vibration control system with maxwell damper in consideration of soil-building interaction," in *Proceedings of Summaries of Technical Papers of Annual Meeting, Architectural Institute of Japan*, pp. 969–970, Sendai, Japan, September 2013, in Japanese.
- [21] T. Koya, K. Shirai, T. Fujimori, K. Ishii, and M. Kikuchi, "Optimum damping characteristic evaluation of vibration control system with hysteretic damper in consideration of soil-structure interaction," in *Proceedings of Summaries of Technical*

- Papers of Annual Meeting, Architectural Institute of Japan*, pp. 681-682, Sendai, Japan, November 2014, in Japanese.
- [22] X. Zhao, S. Wang, D. Du, and W. Liu, "Optimal design of viscoelastic dampers in frame structures considering soil-structure interaction effect," *Shock and Vibration*, vol. 2017, Article ID 9629083, 16 pages, 2017.
- [23] K. Shirai, A. Nagaoka, T. Koya, T. Fujimori, and M. Kikuchi, "Experimental study on optimum damper characteristics of passive control structures considering soil-structure interaction part 1 design of a specimen," in *Proceedings of Summaries of Technical Papers of Annual Meeting, Architectural Institute of Japan*, pp. 13-14, Sendai, Japan, November 2014, in Japanese.
- [24] A. Nagaoka, K. Shirai, T. Fujimori, and M. Kikuchi, "Experimental study on optimum damper characteristics of passive control structures considering soil-structure interaction part 2 methods and results of shake table tests," in *Proceedings of Summaries of Technical Papers of Annual Meeting, Architectural Institute of Japan*, pp. 15-16, Sendai, Japan, November 2014, in Japanese.
- [25] K. Shirai, T. Fujimori, and M. Kikuchi, "Use of shaking table tests to obtain optimal damper characteristics of passive vibration control structures considering soil-structure interaction," in *Proceedings of 16th World Conference on Earthquake Engineering*, Santiago, Chile, January 2017.
- [26] Architectural Institute of Japan, *Seismic Response Analysis and Design of Buildings Considering Dynamic Soil-Structure Interaction*, Architectural Institute of Japan, Tokyo, Japan, 2006, in Japanese.
- [27] The Building Center of Japan, *The Building Standard Law of Japan on CD-ROM May 2016*, The Building Center of Japan, Tokyo, Japan, 2016.
- [28] M. Amin and A. H.-S. Ang, "Nonstationary stochastic model of earthquake motions," *Journal of the Engineering Mechanics Division, ASCE*, vol. 94, no. 2, pp. 559-583, 1968.
- [29] K. Shirai and N. Inoue, "A seismic response estimation method for RC structures using random vibration theory," *Journal of Advanced Concrete Technology*, vol. 12, no. 2, pp. 62-72, 2014.
- [30] M. D. Trifunac and A. G. Brady, "A study on the duration of strong earthquake ground motion," *Bulletin of the Seismological Society of America*, vol. 65, no. 3, pp. 581-626, 1975.

